Journal of Translational Medicine

RESEARCH

Open Access

LncRNA LUCAT1 offers protection against human coronary artery endothelial cellular oxidative stress injury through modulating hsa-miR-6776-5p/LRRC25 axis and activating autophagy flux

Yanjun Wang[1†], Xin Zhang[1†], Mengmeng Ren[1†], Shu He[1], Hengjie Bie[1], Mengyang Duan[1], Zhiyuan Chen[1], Qiaowei Jia[1], Boyu Chi[1], Xiongkang Gan[1], Chengcheng Li[1], Yahong Fu[1], Hanxiao Zhou[1], Sheng Zhang[1], Qian Zhang[1], Fenghui An[3*], Xiumei Chen[2*] and Enzhi Jia[1*]

Abstract

Background Coronary artery disease (CAD) has become a dominant economic and health burden worldwide, and the role of autophagy in CAD requires further clarification. In this study, we comprehensively revealed the association between autophagy flux and CAD from multiple hierarchies. We explored autophagy-associated long noncoding RNA (lncRNA) and the mechanisms underlying oxidative stress-induced human coronary artery endothelial cells (HCAECs) injury.

Methods (1) Autophagy-related proteins including LC3, p62, Beclin1, ATG5, and ATG7 were immunohistochemical stained in coronary specimens; (2) The levels and function of autophagy in the HCAEC oxidative stress model were evaluated using western blot (WB), transmission electron microscopy (TEM), and mRFP-GFP-LC3 adenovirus transfection experiments; (3) The competing endogenous RNA (ceRNA) network of lncRNA LUCAT1/hsa-miR-6776-5p/LRRC25 axis was constructed and validated; (4) The expression levels of above autophagy-related RNAs in peripheral blood mononuclear cells (PBMCs) were verified by qPCR, and their diagnostic performance was subsequently analyzed using receiver operating characteristic (ROC) analysis.

Results (1) The expression of LC3, Beclin1, ATG5, and ATG7 demonstrated a consistent decline whereas p62 expression exhibited an opposite increase as atherosclerosis progressed; (2) Autophagy levels was significantly elevated in HCAECs under oxidative stress, while inhibition of the initial stage of autophagy with 3-MA exacerbated cellular damage; (3) The lncRNA LUCAT1/hsa-miR-6776-5p/LRRC25 axis was established through bioinformatic prediction

†Yanjun Wang, Xin Zhang and Mengmeng Ren have contributed equally to this work.

*Correspondence:
Fenghui An
anfenghui.1975@163.com
Xiumei Chen
cxm2002@126.com
Enzhi Jia
enzhijia@njmu.edu.cn

and validated by dual-luciferase reporter assay, which resulted in a significant decrease in autophagy levels in HCAECs; (4) In total, p62, ATG7, lncRNA LUCAT1 and LRRC25 were validated as robust diagnostic biomarkers for CAD.

Conclusions Our results delineated the dynamic disruption of the autophagy landscape during the progression of human coronary atherosclerosis and identified the lncRNA LUCAT1/hsa-miR-6776-5p/LRRC25 axis, uncovered through transcriptomic profiling, as a protective mechanism against endothelial cell injury through autophagy activation.

Furthermore, we recognized p62, ATG7, lncRNA LUCAT1, and LRRC25 as dependable autophagy-related diagnostic biomarkers in circulating PBMCs, correlating with CAD severity. Collectively, Our findings furnish novel insights into the intricate autophagy landscape at various levels of coronary atherosclerosis and propose potential diagnostic biomarkers, and a theoretical foundation for managing CAD patients.

Keywords Coronary artery disease, Human coronary artery endothelial cell, Oxidative stress, Autophagy flux, LncRNA LUCAT1, Atherogenesis, Diagnostic biomarker

Introduction

Coronary artery disease (CAD), a disease state induced by intima atherosclerotic plaque formation and coronary artery stenosis, remains a leading cause of mortality globally [1]. The interplay of genetic, environmental, and lifestyle factors significantly contributes to the occurrence and development of CAD, leading to a high incidence of CAD [2]. Adverse cardiovascular events like acute myocardial infarction (AMI) and sudden cardiac death (SCD) might happen as the disease progresses. Although clinical therapies have notably enhanced the outcomes for CAD, early diagnosis and intervention remain formidable challenges due to a limited understanding of its pathogenesis and the inadequacy of current diagnostic biomarkers and therapeutic targets, which suffer from low sensitivity and specificity [3].

Autophagy, a crucial molecular pathway for maintaining cellular and organismal homeostasis [4], serves as the primary cellular adaptation mechanism against intra- or extracellular stimuli by engulfing damaged elements and targeting them via lysosomal degradation [5]. Dysregulated autophagy in various vascular cell types, especially in endothelial cells, is widely recognized as a contributing factor in the progression of atherosclerotic plaques. In the initial phase of atherosclerosis, oxidative stress and lipid accumulation induce endothelial cell damage, triggering autophagy as a protective mechanism to stabilize the arterial wall [6]. As autophagic activity diminishes, endothelial cell aging and apoptosis are exacerbated, accompanied by an increased release of inflammatory cytokines and enhanced infiltration of foam cells and macrophages, which collectively promote the progression of atherosclerosis [7, 8]. Although substantial research on autophagy in CAD has been conducted over the years, our understanding of the autophagic landscape in human coronary atherosclerosis remains limited, as does the correlation between autophagy and the severity of coronary atherosclerosis. Besides, the clinical application of autophagy-related findings is still relatively scarce.

LncRNA, a subset of the non-coding RNA family, play critical roles in regulating endothelial cell autophagy through diverse mechanisms affecting gene expression. For instance, LOC107986345 activates endothelial autophagy and inhibits inflammation by enhancing the nuclear translocation of HMGB1via targeting the miR-128-3p/EPHB2 axis [9]. Another study reported that overexpression of lncR-GAS5 suppressed endothelial autophagy through the miR-193-5p/SRSF10 signaling pathway, which was responsible for plaque instability [10]. Additionally, LUCAT1 has been implicated in the regulation of proliferation and apoptosis in cardiomyocytes via targeting miR-181a-5p or miR-612/HOXA13 pathway, thereby contributing to the pathophysiology of AMI and chronic heart failure (CHF) [11, 12]. A Transcriptomic bioinformatics analysis of hepatocellular carcinoma has identified LUCAT1 as a pivotal autophagy-related gene [13]. Nevertheless, the potential alterations in the expression of LUCAT1 in CAD and its involvement in regulating endothelial cell autophagy remain unclear.

In this study, we comprehensively characterized the dynamic autophagy landscape in atherosclerosis associated with CAD through immunohistochemical staining of human coronary atherosclerosis tissues, transcriptome quantification of human PBMCs samples, and RNA sequencing combined with cell culture assays in HCAECs models. Furthermore, the role and targets of lncRNA LUCAT1 in autophagy were elucidated through bioinformatic analysis and in vitro assays, revealing that it activates autophagy through targeting the hsa-miR-6776-5p/LRRC25 axis. Confirmed with the ROC analysis, serveal autophagy-related genes including p62, ATG7, lncRNA LUCAT1, and LRRC25 were identified as novel biomarkers for CAD diagnosis. Collectively, our findings provide new insights into autophagy in CAD, alongside

identifying promising diagnostic biomarkers and potential targets for therapeutic strategies for CAD patients.

Materials and methods

Study designs

We proposed a four-stage design for studying the association between autophagy and CAD, incorporating multiple materials, including tissue, circulating blood samples from the population, along with an oxidative stress cell model. Given the data from the four-stage design, to begin with the validation of the expression levels of autophagy-related proteins in coronary specimens; then the levels and functions of autophagy in HCAECs under oxidative stress were assessed; furthermore, an autophagy-associated ceRNA network involving the lncRNA LUCAT1/hsa-miR-6776-5p/LRRC25 axis was established through comprehensive bioinformatics analysis; finally comes to the validation of auspicious diagnostic biomarkers, along with promising therapeutic targets for CAD strategies in PBMCs. The research design and workflow of the four-stage study are shown in Fig. 1. This study was approved by the ethics committee of Nanjing Medical University and the First Affiliated Hospital of Nanjing Medical University. Written informed consent was obtained from all patients or their authorized representatives in accordance with the principles stated in the Declaration of Helsinki.

Human coronary artery tissues and cell culture

The human coronary artery tissues used in the present study were obtained from four donors at the Department of Human Anatomy at Nanjing Medical University. The bereaved families of the donors provided written informed consent, and the experiments were reviewed and approved by the ethics committees of Nanjing Medical University and the First Affiliated Hospital of Nanjing Medical University. Details of specimen processing were described in our previous studies [14, 15]. Human coronary artery endothelial cells (HCAECs) (Shanghai Honsun Biological Technology Co., Ltd, China) were grown in DMEM/basic medium (Gibco, C11995500BT) supplemented with 10% fetal bovine serum (Gibco, 10270-106). Cells were cultured in an incubator in a humidified atmosphere at 37 °C with 5% CO_2. Cells were digested with 0.25% Trypsin–EDTA (Gibco, 25200-056) and subcultured in the complete medium.

Immunohistochemical staining

A total of 24 coronary segments were enrolled in the immunohistochemical assays. In brief, the sections were deparaffinized, rehydrated, antigen retrieval, and endogenous peroxidase activity blockage before successively incubating with serum, primary antibodies, and then HRP-labeled secondary antibodies. The positive sites were brownish yellow by the DAB solution, and the nucleus was counterstained using hematoxylin. The sections were then dehydrated and visualized under a bright-field microscope. Image-Pro Plus 6.0 software was employed for analysis, with the average integrated optical density (AOD) values of 8 fields of each section calculated. Here is the list of the antibodies: ATG5 (abmart, T55766), ATG7 (abmart, T55658), Beclin1 (abmart, T55092,), LC3 (Servicebio, T55092), p62 (Servicebio, T55092).

Quantitative polymerase chain reaction (qPCR) assay

500 ng of isolated total RNA per sample was capitalized on quantitative PCR analysis. Concisely, the total RNA was extracted and reverse transcribed into cDNA using HiScript® II Q Select RT SuperMix for qPCR (Vazyme, R232-01). The qPCR was performed using Hieff® qPCR SYBR Green Master Mix (Yeasen, 11203ES08) on the QuantStudio 5 system. The relative expression levels of RNAs were calculated by the $2^{-\Delta\Delta ct}$ method and normalized using the expression of the housekeeping gene, GAPDH. Specific primers were provided by GNENray Biotech and listed in Supplementary Table 1.

Cell injury stimulation

The oxidative stress model of HCAECs quest for in vitro study was established via H_2O_2 treatment (0.8 mM, 12 h). A specific concentration was obtained by diluting 3% H_2O_2 solution (Sigma-Aldrich, 88597) with the medium. The autophagy inhibitors 3-MA (5 mM, Selleck, S2767) and CQ (2 μM, Selleck, S6999) were applied by pretreating for 1 h and 2 h before H_2O_2 treatment.

Cell transfection

When HCAECs reached an appropriate confluence at 60–80%, cell transfection was conducted using Lipofectamine 3000 Transfection Reagent (Invitrogen, USA) following the manufacturer's protocol. Small interfering RNAs (siRNAs) of lncRNA LUCAT1 and negative control (si-NC) were applied in the present study.

Cell counting Kit-8 (CCK8) assays

The cell viability was confirmed with Cell Counting Kit (Yeasen, 40203ES60). Briefly, HCAECs were seeded in 96-well plates at 5×10^3 cells / well with 8 parallel wells in each group. After cell treatments, 10 μl CCK8 solution was added to each well and incubated for 2.5 h. A microplate reader was used to measure the optical density (OD) values.

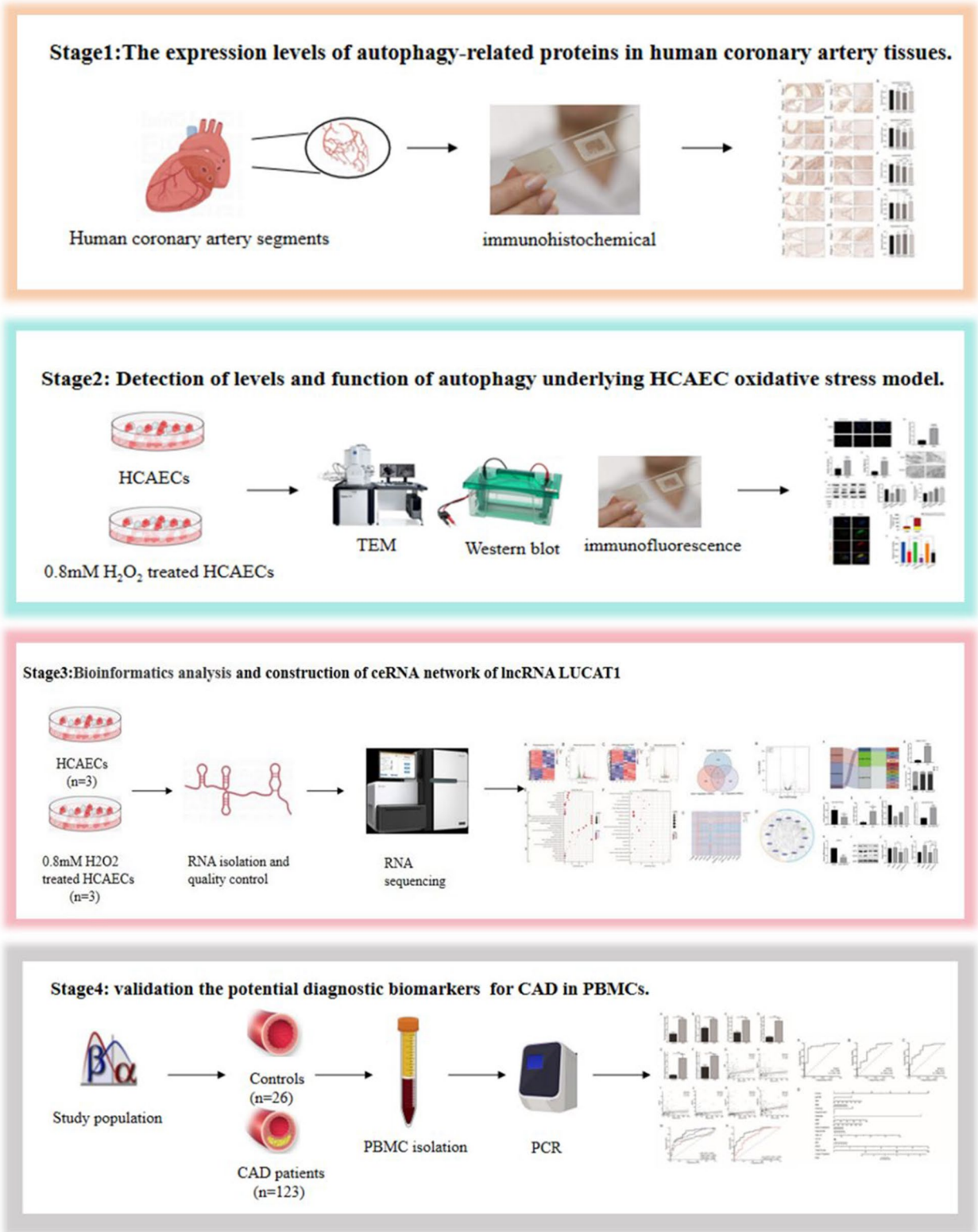

Fig. 1 The research design and workflow of the four-stage study. The validation of the expression levels of autophagy-related proteins in human coronary artery tissues (stage 1). Detection of levels and function of autophagy in oxidative stress-induced human coronary artery endothelial cells (HCAEC) model (stage 2). Bioinformatics analysis and construction of ceRNA network of lncRNA LUCAT1/hsa-miR-6776-5p/LRRC25 axis (stage 3). The validation of diagnostic biomarkers and therapeutic targets for CAD in peripheral blood mononuclear cells (PBMC) (stage 4)

Intracellular ROS detection

The levels of intracellular oxidative stress were measured using a reactive oxygen species (ROS) Assay Kit (Beyotime, S0033). Cells were in-situ loaded with DCFH-DA at 10 μM diluted in 100 μl serum-free medium per well. After 20 min of dark incubation, the nucleus was stained for 5 min with Hoechst (Beyotime, C1027), followed by inverted fluorescence microscope observation.

Transmission electron microscope (TEM)

Intracellular autophagic ultrastructures were observed by transmission electron microscopy (TEM) in the absence or presence of H_2O_2. In a nutshell, abundant cells were harvested and fixed with TEM fixative, followed by agarose pre-embedding, 1% OsO4 post-fixing, ethanol gradient dehydration, acetone soak, resin penetration and embedding, polymerization, and staining. Finally, the section images were acquired under a transmission electron microscope.

Western blot

Total proteins in HCAECs were obtained using RIPA lysis buffer (Beyotime, P0013B) containing 1% phenylmethanesulfonyl fluoride (PMSF, Beyotime, ST506), and concentration was measured. Proteins were separated in the SDS-PAGE gel and transferred to the PVDF membrane. The target protein bands were visualized by the enhanced chemiluminescence (ECL) system kit (Vazyme, E412-01) after stepwise antibodies incubation. β-actin was used as a loading control to standardize protein levels. Quantitative analysis of immunoblot bands was performed on ImageJ software. The antibodies enrolled in this study were LC3B (1:1000, abmart, T55992), p62 (1:1000, abmart, T55546), β-actin (1:2000, abmart, P60035), and goat-anti-Rabbit IgG (1:10000, zsbio, 711-035-152).

Confocal microscope

The stubRFP-sensGFP-LC3 Adenovirus (Shanghai Gnenchem) was commissioned in our present study. Cells planted in a confocal dish were transfected with mRFP-GFP-LC3 adenovirus (multiplicity of infection, MOI = 100) when it reached a confluence of 40–50%. During 36–48 h after transfection, cells were observed under a laser scanning confocal microscope and acquired images. For quantitative analysis, yellow puncta (autophagosomes) and red-only puncta (autolysosomes) were counted using Image J, and 50 cells per group from 3 to 5 independent experiments were enrolled.

RNA sequencing, and data preprocessing

The rRNA-depleted RNA sequencing between the control group (n = 3) and the H_2O_2 group (n = 3) was then performed in the present study. In brief, 1 μg of each sample satisfied with RNA Integrity Number (RIN) ≥ 7 was enrolled in library construction. The size and purity of libraries were validated before sequencing was processed on the Illumina sequencing platform (HiSeqTM 2500). Subsequently, we filtered high-quality reads from raw sequencing data, on which all subsequent analyses were based. By excluding adapters and low-quality bases and inspecting the quality of Q30 and GC content using fastqc, clean reads were obtained. Alignment, assembly, and quantification were achieved using hisat2 and Stingtie.

LncRNA identification

The mining of prospective lncRNAs was conducted with a rigorous four-step procedure. Firstly, CuffCompare was used to screen out both known coding transcripts and novel transcripts of known motifs. Secondly, we eliminated transcripts with a single exon or ≤ 200 nt in length. Thirdly, algorithms, including CPC, CNCI, Pfam, and PLEK, were utilized to predict the protein-coding potential of lncRNA, and we retained the intersection of transcripts without coding potential. Fourthly, aligning the candidate lncRNA sequences by blastn to distinguish known lncRNA and novel lncRNA.

Differential analysis of mRNA and lncRNA

The differential expression (DE) analysis was conducted between two groups. The matched reads counts obtained by bowtie2 alignment were normalized in an FPKM manner. Screening DEmRNAs and DElncRNAs was achieved using DESeq2 R package with thresholds of |log2 FC |> 1 and adjusted $p < 0.05$. Transcripts that met the criteria were visualized using ggplot2 and ComplexHeatmap in R.

Functional enrichment analysis

Gene Ontology (GO) and Kyoto Encyclopedia of Genes and Genomes (KEGG) pathway analysis were performed on DEmRNAs using the clusterProfiler R package. We visualized the top enriched results of both KEGG pathways and GO terms, including molecular function (MF), cellular component (CC), and biological process (BP). Significance criteria of adjusted $p < 0.05$ were applied to all enrichment procedures.

Protein–protein interaction (PPI) network and hub genes identification

We established a PPI network of DEmRNAs using the STRING database (https://string-db.org/), and protein pairs with an interaction score > 0.9 were selected for visualization. The Cytoscape software was utilized to visualize the PPI network by MCODE. In addition, we employed the cytoHubba plugin of Cytoscape to select

hub genes in PPI network. The intersection of seven algorithms, including MNC, MCC, EPC, DMNC, Closeness, Radiality, and Betweenness, were identified as hub genes.

LncRNA-miRNA analysis and ceRNA network construction

We then constructed a lncRNA-miRNA-mRNA network dedicated to exploring potential ceRNA regulatory relations. The lncRNA-miRNA pairs were obtained using miranda. A network diagram was generated for the top 300 lncRNA-miRNA pairs with the smallest *p*-value. Then, we obtained the lists of predicted target mRNA by subjecting the most enriched miRNA to three databases. The intersection of miRDB, miRWalk, and TargetScan results, apart from non-differentially expressed mRNA, served as candidates for miRNA-mRNA pairs construction. Ultimately, the Cytoscape was used to establish the ceRNA regulatory network of lncRNA-miRNA-mRNA.

Co-expression of autophagy-associated DEmRNAs and DElncRNAs

The list of autophagy genes was derived from The Human Autophagy Database (HADb, http://autophagy.lu/clustering/index.html), and a Venn diagram was applied to obtain autophagy-associated DEmRNAs**.** We performed the Pearson correlation analysis based on the rcorr () in the Hmisc R package to explore DElncRNAs co-expressed with autophagy-associated DEmRNAs. The significant coexpression criteria were Pearson correlation coefficient $|r|>0.95$ and $p<0.01$. Eventually, Cytoscape software was applied to visualize the co-expression network.

Cytoplasmic/Nuclear fractionation assay

The RNA components of the cytoplasm and nucleus were separated using the Cytoplasmic and Nuclear RNA Purification Kit (Norgen Biotek, 21000). HCAECs were lysed in ice-cold Lysis Buffer J and centrifuged. Then, Buffer SK and 100% ethanol were added to the supernatant containing cytoplasmic RNA and the pellet containing nuclear RNA. Vortexing and centrifuging were performed to bind cytoplasmic and nuclear RNA to the spin column. After washing, RNA was purified and eluted finally. The levels of cytoplasmic and nuclear RNA and the efficiency of purification experiments were verified by qPCR.

Dual-Luciferase reporter assay

The relationship between LUCAT1 and hsa-miR-6776-5p, as well as hsa-miR-6776-5p and LRRC25, was probed using dual-luciferase reporter assays. The report vectors of 3'UTR mutant (- MUT) and wild type (- WT) of LUCAT1 and LRRC25 were constructed in the present study. HEK-293 T cells were seeded to 96-well plates and the vectors were co-transfected with hsa-miR-6776-5p mimics or hsa-miR-6776-5p negative control (NC) once the cells reached the appropriate density. After 48 h of co-transfection, the following steps were performed using Dual-Luciferase reporter system (Hanbio Biotechnology) according to the manufacturer's instructions. The relative luciferase activity was calculated after normalizing to firefly luciferase activity.

Study population

In the present study, subjects were recruited from the First Affiliated Hospital of Nanjing Medical University from July 2022 to March 2023 and were grouped based on coronary angiography results. Specifically, participants with stenosis > or = 50% in at least one major coronary artery were defined as CAD subjects, while those with stenosis < 50% in major coronary arteries were defined as control subjects [16]. Subjects with the following conditions were excluded: congenital heart defects, cardiomyopathy, cerebrovascular diseases, type 1/2 diabetes, malignant tumors, severe bacterial/virus/fungi infection, severe hepatic insufficiency, and renal insufficiency. A total of 123 CAD subjects and 26 healthy controls were enrolled in our study. A Gensini score was calculated for each subject to indicate the degree of coronary artery stenosis [17]. Clinical data, including medical history (age, gender, smoking history, alcohol intake, heart rate, and blood pressure) and laboratory parameters (C-reactive protein, total cholesterol, triglyceride, high-density lipoprotein cholesterol, low-density lipoprotein cholesterol, and lipoprotein a) were abstracted from their medical records as available.

PBMCs isolation and RNA extraction

Using a lymphocyte separation medium (TB500, Tianjin, China), PBMCs were isolated from circulating blood samples collected from CAD subjects and healthy controls within 4 h of sample collection. Total RNA extraction was conducted using Trizol Reagent (Vazyme, R401-01) following the manufacturer's instructions. RNA samples with an A260/A280 value (the ratio of the absorbance at 260 and 280 nm) in the 1.8–2.0 range and an appropriate concentration, both measured by NanoDropOne® spectrophotometer, were capable of subsequent expression validation experiments.

Statistical analysis

Data were analyzed by GraphPad Prism (version 8.0) and presented in the format of mean ± standard deviation (SD), median (lower quartile, upper quartile), or number out of number (n/n). For continuous variables that satisfied normal distribution and homogeneity of variables, an unpaired two-tailed Student's t-test was applied to compare the difference between two groups, while one-way

ANOVA was applied among three or more groups comparison. The Mann–Whitney U test was applied for abnormally distributed continuous variables. Categorical data were compared using the chi-square test. Receiver operating characteristic (ROC) curves were applied to determine the diagnostic values of mRNAs and lncRNA combined with the area under the curve (AUC), specificity, sensitivity, Youden index, and cut-off values for CAD. Spearman correlation analyses were applied to verify the relationship between mRNAs and lncRNA and clinical characteristics. A $p < 0.05$ was accepted to be statistically significant.

Results

Autophagy-related proteins in different pathologic stages of coronary atherosclerosis

We first focus on the dynamic changes in autophagy levels during the pathological progression of coronary atherosclerosis. We employed microtubule associated protein 1 light chain 3 (LC3), sequestosome 1 (SQSTM1/p62), Beclin1/BECN1, autophagy related 5 (ATG5), and autophagy related 7 (ATG7) as immunohistochemical markers and analyzed the staining results of those autophagy-related proteins in a relative AOD values manner. A total of 24 complete coronary artery specimens were enrolled, comprising 4 from stage 1 (fatty streak tunica intima), 6 from stage 2 (fibrous plaques tunica intima), and 7 each from stage 3 (atherosclerotic tunica intima) and 4 (secondary affection tunica intima). The histological classification of all atherosclerotic lesions was previously validated by H&E staining in our previous studies [14, 15]. Of all atherosclerosis lesions, the highest expression of LC3, Beclin1, and ATG5 was identified in stage 1 atherosclerotic lesions, followed by a consistent and significant decline as the disease progressed. Notably, a slight increase in LC3 and Beclin1 expressions was seen from stage 3 to stage 4 (Fig. 2A–F). The expression of ATG7 is down-regulated in stage 3 and up-regulated in stage 4, compared to stage 1. However, no significant differences of ATG7 expression were detected between stage 1 and 2 (Fig. 2G, H). Conversely, p62 expression displayed an increasing trend from stage 1 to stage 4, with a minor decrease noted in stage 4 (Fig. 2I, J). An additional summary of autophagy-related protein expression among pathologic stages is available in the supplementary Table 2. Altogether, our findings indicate a close association between disrupted autophagy and the progression of atherosclerosis, suggesting a fundamental role in expediting atherosclerosis progression.

Autophagy flux elevated in HCAECs oxidative stress model

Oxidative stress damage in HCAECs is momentous in the initiation and progression of coronary atherosclerosis. By comparing the relative fluorescence intensities between the two groups, we found that cells treated with H_2O_2 displayed significant elevation in intracellular ROS levels compared to the control group (Fig. 3A, B). LDH and MDA assays were utilized to evaluate cellular oxidative stress levels and cell viability, and the results showed that LDH and MDA levels were significantly elevated in the H_2O_2-treated group compared to the control group (Fig. 3C, D). Collectively, the oxidative stress model of HCAECs was established. Furthermore, the changes in autophagy levels under oxidative stress were assessed. From the perspective of visually observing the intracellular ultrastructure, TEM assay showed a considerable amount of autophagic vesicles in H_2O_2-treated cells, including autophagosomes and autolysosomes (Fig. 3E). Subsequently, the autophagy flux was blocked at an early stage with 3-MA or at a late stage with CQ. The ratio of LC3 II/I, a typical indicator of autophagy, was significantly increased in the H_2O_2 group and CQ + H_2O_2 group (Fig. 3F–H). Additionally, p62 accumulation was observed in the late-stage autophagy blockade group compared to the H_2O_2 treatment groups, with or without early-stage autophagy blockade (Fig. 3G). Moreover, the dynamic process of intracellular autophagy was monitored through mRFP-GFP-LC3 adenovirus transfection. By incorporating mRFP and GFP genes into the same vector with LC3, the fluorescent signals enable precise intracellular tracking of LC3. Under normal conditions, mRFP produces red fluorescence, GFP generates green fluorescence, and their overlapping fluorescence emits a yellow signal [18]. Using confocal microscopy, we observed an increase in the number of autolysosomes ($mRFP^+$ and GFP^-) and autophagosomes (merged $mRFP^+$ and GFP^+), with a greater expansion in autolysosomes. Since the green fluorescence is quenched during autophagosome-lysosome fusion in acidic

(See figure on next page.)

Fig. 2 The expression of the autophagy-related proteins, LC3, p62, Beclin1, ATG5, and ATG7 in different stages of atherosclerosis analyzed by immunohistochemical assay. The expression level and bar chart of LC3 (**A**, **B**), Beclin1 (**C**, **D**), ATG5 (**E**, **F**), ATG7 (**G**, **H**), and p62 (**I**, **J**) in all stages of atherosclerosis (stage 1 n = 4, stage 2 n = 6, stage 3 n = 7, stage 4 n = 7). Stage 1: fatty streak tunica intima; Stage 2: fibrous plaques tunica intima; Stage 3: atherosclerotic tunica intima; Stage 4: secondary affection tunica intima. Low magnification 100×. Scale bar: 200 μm. High magnification 400×. Scale bar: 50 μm. *$P < 0.05$, **$P < 0.01$, ***$P < 0.001$, ****$P < 0.0001$

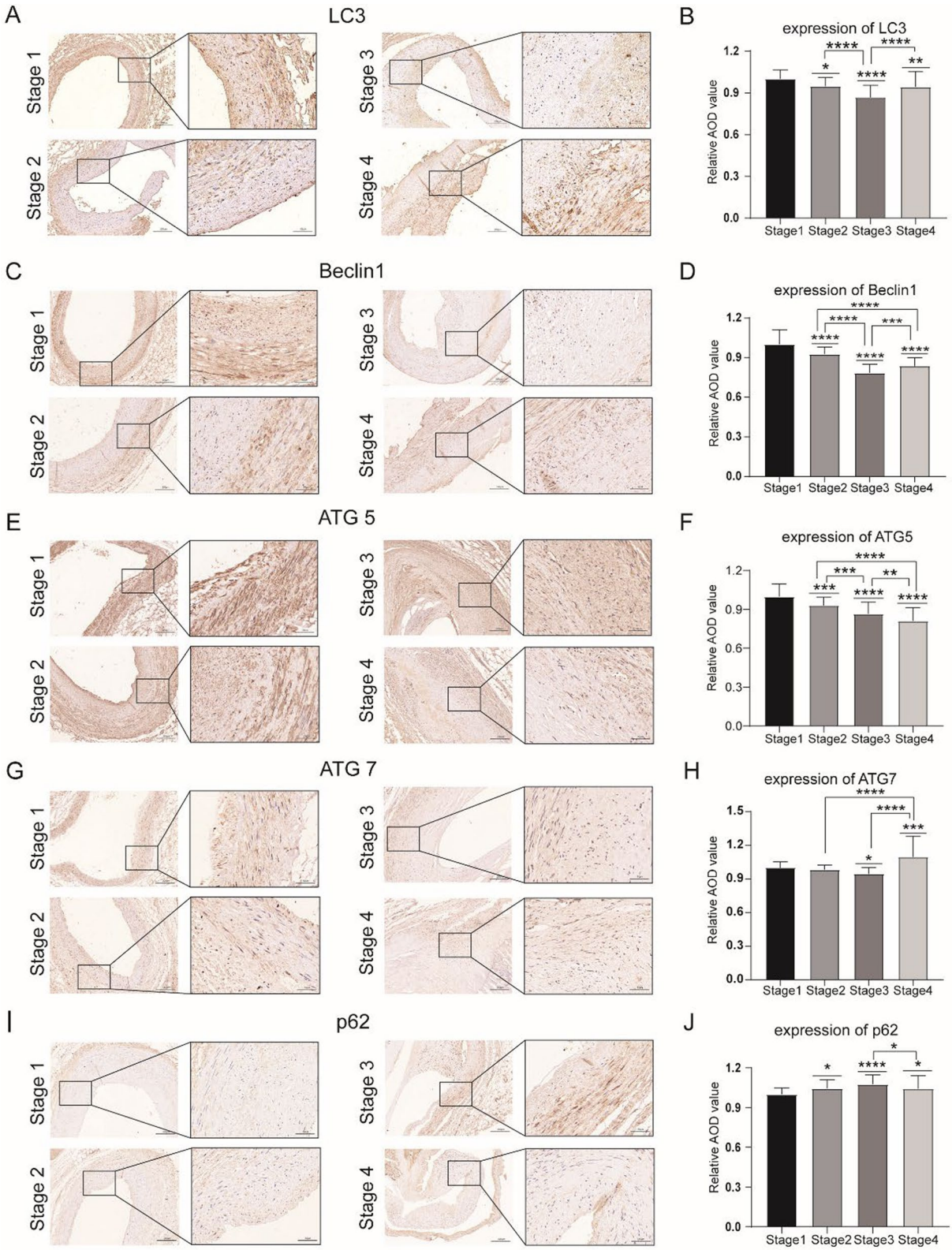

Fig. 2 (See legend on previous page.)

environments, the reslut suggesting that the acidic autolysosomes were piled up (Fig. 3I, J). The above results indicated an elevated fluent autophagy induced by oxidative stress in HCAECs. Additionally, cell viability, quantified using the CCK8 assay, was significantly decreased in the 3-MA + H_2O_2 group, emphasizing the critical role of early-stage autophagy in mitigating oxidative stress-induced damage. In contrast, blocking the late stage of autophagy neither alleviated nor worsened overall cell damage (Fig. 3K). Thus, we determined that a vibrant level of autophagy contributes to defending against endothelial injury under oxidative stress, suggesting the protective function of autophagy.

Identification of DEmRNAs and DElncRNAs and functional enrichment analysis

Whole-transcriptome sequencing was then performed comparing the control group (n = 3) and the H_2O_2 group (n = 3) to disclose RNAs associated with oxidative stress response in HCAECs. Principal component analysis (PCA) of the lncRNA transcriptome revealed distinct clustering of samples from the control and the H_2O_2 groups, with the first two principal components explaining 30.62% and 19.2% of the total variance, respectively (Supplemental Fig. 1A, B). We identified 795 DEmRNAs and 208 DElncRNAs meeting the cutoff criteria of $|\log_2 FC| > 1$ and adjusted $p < 0.05$, as visualized using heat mapping (Fig. 4A, C). As shown in the volcano plot, 470 mRNAs and 83 lncRNAs were upregulated, whereas 325 mRNAs and 125 lncRNAs were downregulated (Fig. 4B, D). The biological functions of DElncRNAs were characterized by GO and KEGG pathway analysis. Given that cis-regulation is common in lncRNA function exerting, the lncRNAs functional annotation was achieved by their neighboring genes evaluating [19]. Of great notice, ferroptosis, PI3K-Akt signaling pathway, and mTOR pathway in KEGG pathway and lysosome term and lysosomal membrane term in CC module in GO analysis displayed a prominent enrichment among upregulated lncRNAs (Fig. 4E, F). Functional enrichment results for downregulated lncRNAs were shown in Supplemental Fig. 1C, D. Those findings underscored the prospective significant role of a panel of differentially expressed lncRNAs in regulating intracellular autophagy under oxidative stress.

PPI, ceRNA network construction and hub genes identification

Upon analyzing DEmRNAs in the STRING database, a protein–protein interaction (PPI) network with the highest score of 26.667 was then extracted using the MCODE plugin in Cytoscape (Supplementary Fig. 2A). In the ranked order following were modules 2–5 (Supplementary Fig. 2B). Utilizing seven algorithms within the cytoHubba plugin, 13 hub genes were identified: CDC20, TOP2A, KIF20A, DLGAP5, PLK1, AURKA, CEP55, CENPE, CCNB2, CDCA8, NDC80, KIF23, and CCNA2, with their intersections shown in an upset diagram (Supplementary Fig. 2C). The top 15 node interactions, ranked by MCC, were then illustrated (Supplementary Fig. 2D). Additionally, the top 300 lncRNA-miRNA pairs, predicted by Miranda with the lowest *p*-values, were mapped, involving 186 DElncRNAs and 11 miRNA targets (Supplementary Fig. 3A). The predicted mRNA targets of these projected miRNAs were generated from an overlapping dataset from miRDB, TargetScan, and miRWalk databases, as well as the DEmRNAs list. Consequently, a total of 165 DElncRNAs (74 downregulated and 91 upregulated), 6 miRNAs, and 17 DEmRNAs (8 downregulated and 9 upregulated) were incorporated into the ceRNA network. This ceRNA network, consisting of 221 lncRNA-miRNA pairs and 19 miRNA-mRNA pairs, was visualized using Cytoscape (Supplementary Fig. 3B), highlighting the potential regulatory mechanisms underpinning the oxidative stress response in HCAECs.

Identification of autophagy-associated DElncRNAs and co-expression analysis

The 222 autophagy-associated genes were derived from The Human Autophagy Database (http://www.autophagy.lu/clustering/index.html) online. By comparing the obtained database with the list of differentially expressed genes in HCAECs, 11 upregulated and 1 downregulated autophagy-associated genes were extracted using a Venn diagram (Fig. 5A). A volcano plot based on sequencing data was utilized to

(See figure on next page.)

Fig. 3 Detection of autophagy in oxidative stress-induced HCAECs injury. **A**, **B** Intracellular ROS level was studied by ROS analysis. Scale bar: 50 μm; **C** LDH assay; **D** MDA assay; **E** TEM analysis. Arrows indicate autolysosomes and/or lysosomes. Scale bar: low magnification: 5.0 μm, high magnification: 1.0 μm; **F**–**H** relative expression of autophagy proteins detected by western blot; **I**, **J** autophagy flux accessed by mRFP-GFP-LC3 adenovirus transfection assay. Red puncta ($mRFP^+$ and GFP^-), autolysosomes; yellow puncta (merged $mRFP^+$ and GFP^+), autophagosomes. Scale bar: 10 μm; **K** cell viability measured after upstream and downstream autophagy blockage by CCK8 assay. TEM: transmission electron microscopy; 3-MA: 3-Methyladenine; CQ: chloroquine. **P < 0.05, **P < 0.01, ****P < 0.0001*

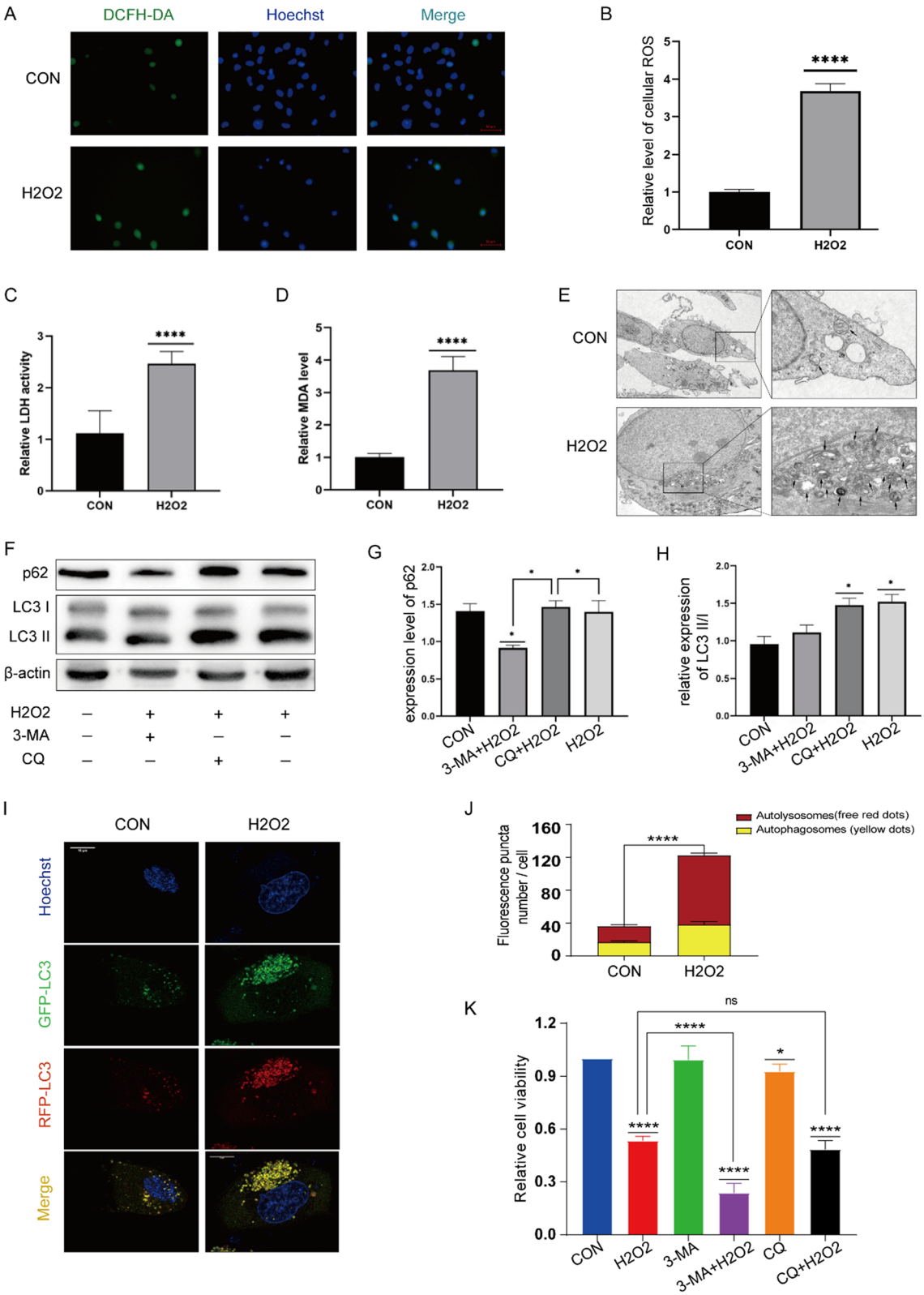

Fig. 3 (See legend on previous page.)

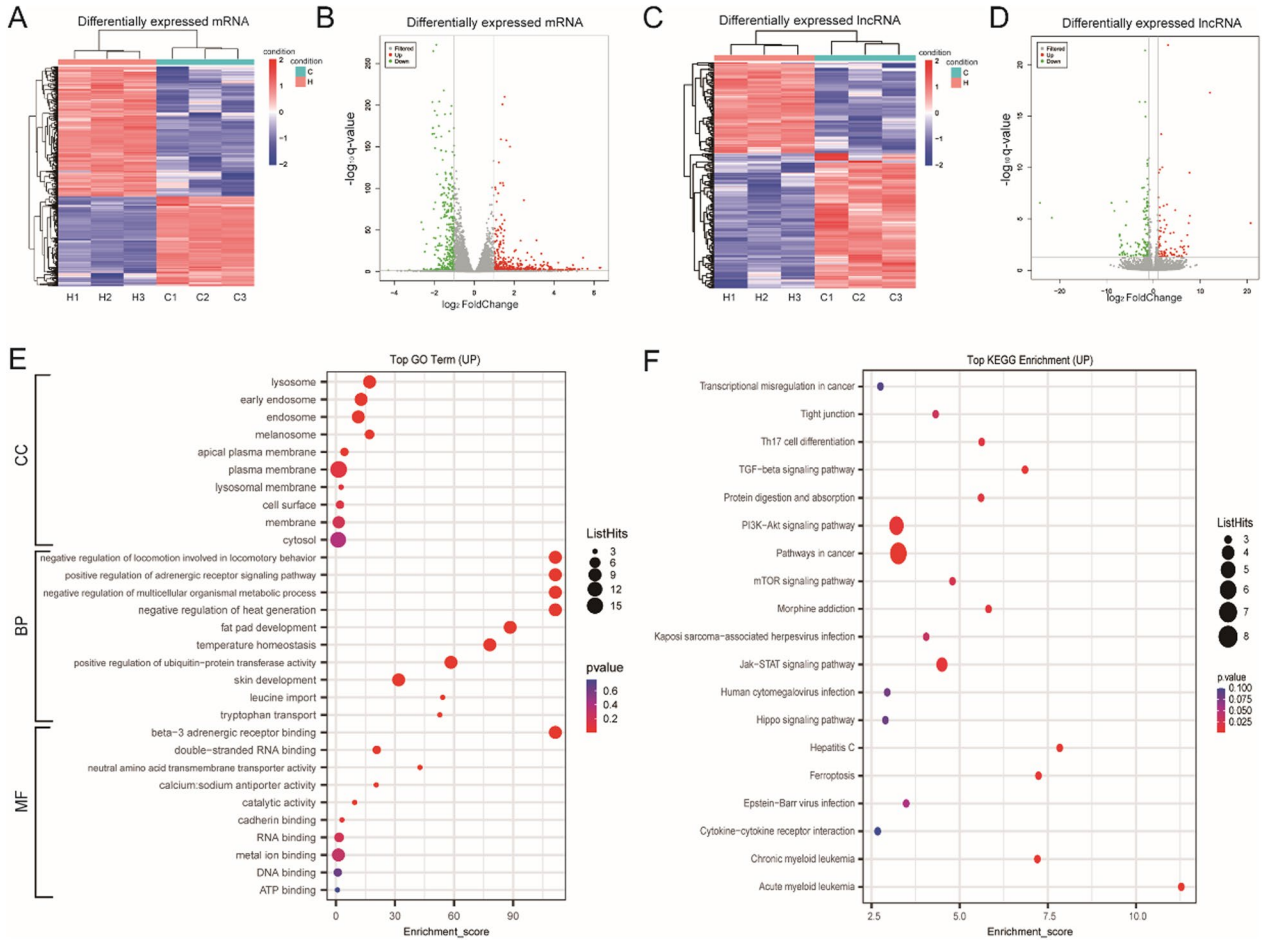

Fig. 4 Identification of DEmRNAs and DElncRNAs and functional enrichment analysis. A cluster heat map of DEmRNAs (**A**), a volcano map of DEmRNAs (**B**), a cluster heat map of DElncRNAs (**C**), and a volcano map of DElncRNAs (**D**) between the CON group (n = 3) and H2O2 group (n = 3) in HCAECs. The top 30 enriched terms associated with the BP, CC, and MF in GO analysis (**E**) and the top 20 enriched KEGG pathways (**F**) of up-regulated DElncRNAs. DEmRNAs: differentially expressed mRNAs; DElncRNAs: differentially expressed lncRNAs; GO: Geno Ontology; BP: biological process; CC: cellular component; MF: molecular function; KEGG: Kyoto Encyclopedia of Genes and Genomes

characterize the expression of all autophagy-associated genes under oxidative stress conditions in HCAECs (Fig. 5B). To identified autophagy-associated lncRNAs, Pearson correlation analysis was performed. The co-expression relationship between autophagy-associated DEmRNAs and DElncRNAs was visualized with a heat map based on the correlation scores (Fig. 5C). LncRNAs with a high coefficient $|r| > 0.95$ and $p < 0.01$ were categorized as autophagy-associated lncRNAs. Ultimately, 76 differentially expressed autophagy-associated lncRNAs were identified, including 43 downregulated and 33 upregulated lncRNAs. The co-expression network including 211 mRNA-lncRNA pairs was shown using Cytoscape (Fig. 5D).

Construction and verification of ceRNA network of lncRNA LUCAT1

In our preliminary study, three variant transcripts of the lncRNA LUCAT1 (ENST00000648015, ENST00000650047, and ENST00000649467) were identified as differentially expressed and associated with autophagy, using the Ensembl database (https://asia.ensembl.org/index.html) (Supplementary Fig. 3A). The biological functions of LUCAT1 were then investigated using bioinformatics analysis. GO enrichment analysis highlighted LUCAT1's involvement in lysosomal processes (GO:0005764), suggesting its potential role in autophagy-regulated atherosclerosis development. Based on our ceRNA network analysis (Supplementary Fig. 3B),

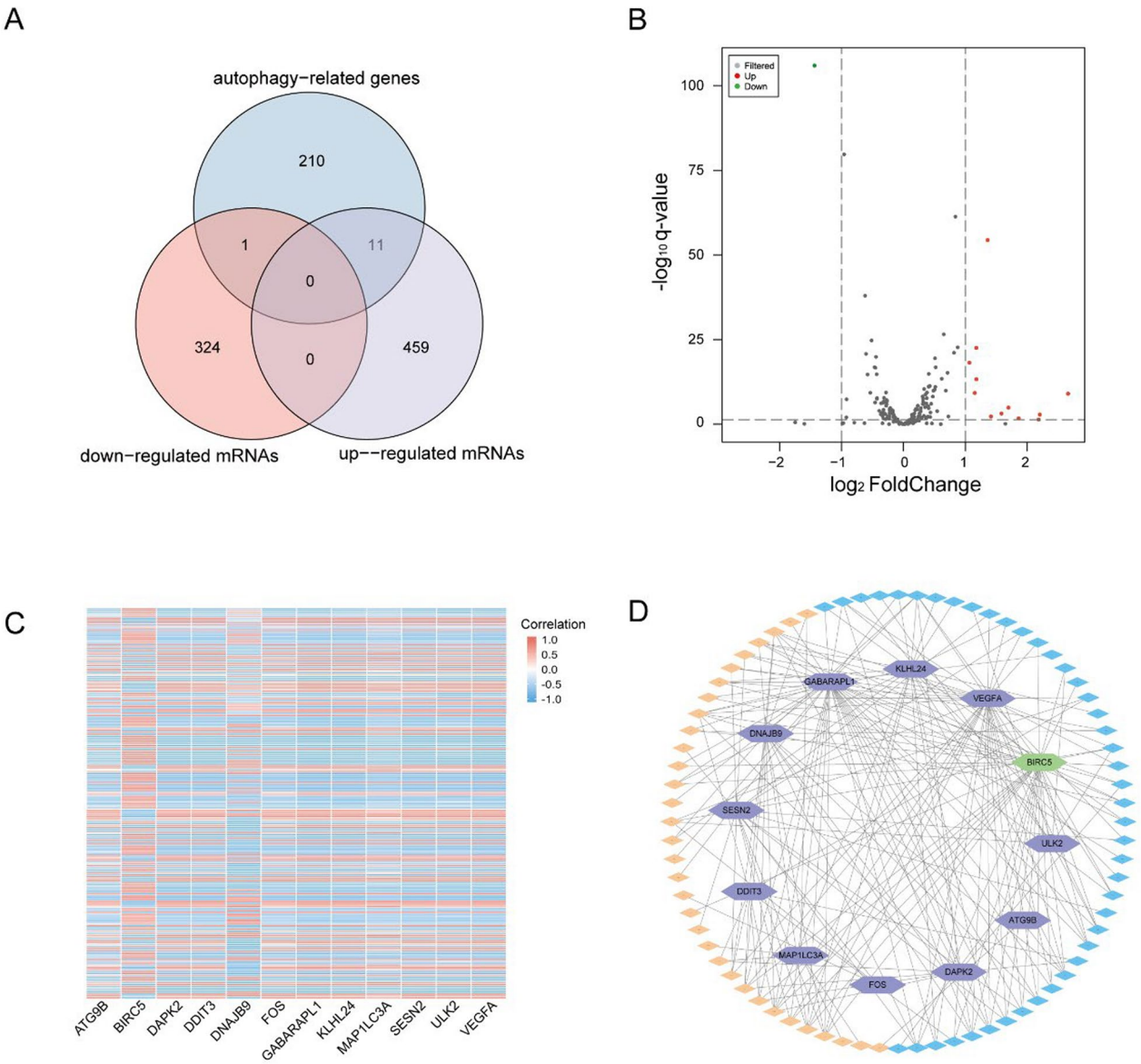

Fig. 5 Identification of autophagy-associated DElncRNAs and co-expression analysis. **A** The intersection of autophagy-related genes, down-regulated mRNAs, and up-regulated mRNAs; **B** a volcano map of autophagy-associated genes; **C** a heat map of the correlation between autophagy-associated DEmRNAs and DElncRNAs; **D** co-expression network of autophagy-associated DEmRNAs and DElncRNAs. The blue rhombus indicates down-regulated lncRNAs, the orange rhombus indicates up-regulated lncRNAs, the green polygon indicates down-regulated mRNAs, and the bluish violet polygon indicates up-regulated mRNAs. DEmRNAs: differentially expressed mRNAs; DElncRNAs: differentially expressed long noncoding RNAs

we derived the LUCAT1-related ceRNA networks, where three LUCAT1 transcripts regulate 11 mRNAs by targeting 3 miRNAs: hsa-miR-619-5p, hsa-miR-1273 h-5p, and hsa-miR-6776-5p (Fig. 6A).

The quantification of LUCAT1 expression was achieved by qPCR, and the results demonstrated a significant upregulation of LUCAT1 in HCAECs under oxidative stress (Fig. 6B). Notably, LUCAT1 was predominantly localized in the nucleus(Fig. 6C), suggesting that it might be involved in the dynamic progress of autophagy in response to the HCAECs injury through both transcriptional and post-transcriptional mechansims. Given that LRRC25 is recognized as an autophagy-related molecular scaffold facilitating the p62-dependent degradation of autophagosomes [20], we further investigated whether LUCAT1 could modulate autophagy through hsa-miR-6776-5p/LRRC25 axis in HCAECs. Conversely, the

expression of hsa-miR-6776-5p was downregulated, whereas LRRC25 expression was upregulated under conditions of oxidative stress (Fig. 6D, E). The binding sites between LUCAT1 and hsa-miR-6776-5p, as well as between hsa-miR-6776-5p and LRRC25, were predicted online. As illustrated in the schematic, two predicted binding sites for hsa-miR-6776-5p were identified in the LUCAT1 and LRRC25 sequences, respectively. Dual-luciferase reporter assays were conducted using recombinant plasmids containing either wild-type (-WT) or mutant (-MUT) sequences of the target genes in HEK-293 T cells to elucidate the predicted binding interactions, with the -WT plasmids harboring mutations at both predicted binding sites (Fig. 6F, G). A significant reduction in luciferase activity was detected when LUCAT1-WT and hsa-miR-6776-5p mimics were co-transfected, compared with the LUCAT1-MUT group (Fig. 6H). Similarly, the luciferase activity in the LRRC25-WT group was notably reduced following hsa-miR-6776-5p mimics interference, whereas the mutant sequences of LRRC25 exhibited no notable difference (Fig. 6I). To further verify the targeted regulated relationship among this intracellualr axis, a knockdown system for LUCAT1 was established using siRNA, with efficiency validated by qPCR. The qPCR results showed that the depletion of LUCAT1 resulted in the upregulation of hsa-miR-6776-5p and the downregulation of LRRC25 in HCAECs (Fig. 6J). Collectively, our findings established the interactive association that lncRNA LUCAT1 may regulate LRRC25 expression by sponging hsa-miR-6776-5p. Furthermore, autophagy assessment showed a significant decrease in the LC3 II/I ratio in LUCAT1-knockdown cells compared to controls, without notable changes in p62 expression (Fig. 6K–M). These findings indicate that LUCAT1 knockdown hinders autophagy activation under oxidative stress, underscoring its regulatory function in autophagy and potential impact on atherosclerosis development.

Evaluation of autophagy-related RNAs as CAD diagnostic biomarkers

Sequential cohorts were enrolled to investigate the distribution patterns of autophagy-related RNAs in CAD. The demographic characteristics and clinicopathological data of each subject were summarized in Supplementary Table 3 and Supplementary Table 4, respectively. Significant differences were observed in gender, hypertension, total cholesterol, and Gensini scores between healthy controls and CAD patients ($p < 0.05$). The expression of p62, Beclin1, ATG5, ATG7, lncRNA LUCAT1, and LRRC25, relative to GAPDH, were significantly increased in CAD patients compared to healthy controls (Fig. 7A–F) (Supplementary Table 5 and Supplementary Table 6). Noteworthy mentioning that LC3 data were excluded from statistical analysis due to excessively high CT values. Spearman correlation analysis revealed positive correlations between Gensini scores and the expressions of p62 ($R = 0.337$, $p < 0.001$), ATG7 ($R = 0.310$, $p < 0.001$), lncRNA LUCAT1 ($R = 0.435$, $p < 0.001$), and LRRC25 ($R = 0.196$, $p = 0.031$) (Fig. 7G, J–L). No significant correlation was found between Beclin1 expression and CAD severity ($R = 0.142$, $p = 0.084$), while a slight positive correlation existed for ATG5 ($R = 0.172$, $p = 0.036$) (Fig. 7H, I).

ROC curve analysis evaluated CAD diagnostic performance, revealing AUC values for p62 (0.830), Beclin1 (0.653), ATG5 (0.666), and ATG7 (0.799) (Fig. 7M) (Supplementary Table 7). This analysis identified p62 and ATG7 as efficient CAD biomarkers, with sensitivities of 0.911 and 0.678 and specificities of 0.654 and 0.846, respectively. The AUCs for lncRNA LUCAT1 (0.869) and LRRC25 (0.748), along with their sensitivities (0.814 and 0.598) and specificities (0.792 and 0.792), further underscored their diagnostic utility (Fig. 7N). Overall, p62, ATG7, lncRNA LUCAT1, and LRRC25 were identified as effective diagnostic biomarkers for CAD. Furthermore, three diagnostic models were developed incorporating CRP, lipid parameters (triglycerides and HDL-C), and either p62 (model I), ATG7 (model II), or both p62 and

(See figure on next page.)

Fig. 6 Construction and verification of ceRNA network of lncRNA LUCAT1/hsa-miR-6776-5p/LRRC25. **A** The Sankey plot of lncRNA LUCAT1-miRNA-mRNA interaction; **B** the expression levels of lncRNA LUCAT1 between the control group and H_2O_2-treated group, measured by qPCR; **C** the subcellular localization of lncRNA LUCAT1 was quantified by qPCR, using GAPDH as the cytoplasmic reference gene and U6 as the nuclear reference gene. nuc, nucleus; cyto, cytoplasm; **D**, **E** the expression levels of hsa-miR-6776-5p and LRRC25 between the control group and H_2O_2-treated group; **F** two complementary binding of hsa-miR-6776-5p and wild/mutant type of LUCAT1; **G** two complementary binding of hsa-miR-6776-5p and wild/mutant type of LRRC25; **H** the luciferase activity of the reporter vectors containing wild type or mutant LUCAT1 sequences after co-transfected with hsa-miR-6776-5p or hsa-miR-NC in HEK 293 T cells; **I** the luciferase activity of the reporter vectors containing wild type or mutant 3'UTR sequence of LRRC25 after co-transfection with hsa-miR-6776-5p or hsa-miR-NC in HEK 293 T cells; **J** the expression levels of hsa-miR-6776-5p and LRRC25 in lncRNA LUCAT1 knockdown system using siRNAs specific to LUCAT1; **K**–**M** the expression levels of autophagy-related proteins, LC3 and p62, in HCAECs under oxidative stress in the presence of LUCAT1 knockdown. ceRNA: competitive endogenous RNA. *$P < 0.05$, **$P < 0.01$, ***$P < 0.001$, ****$P < 0.0001$

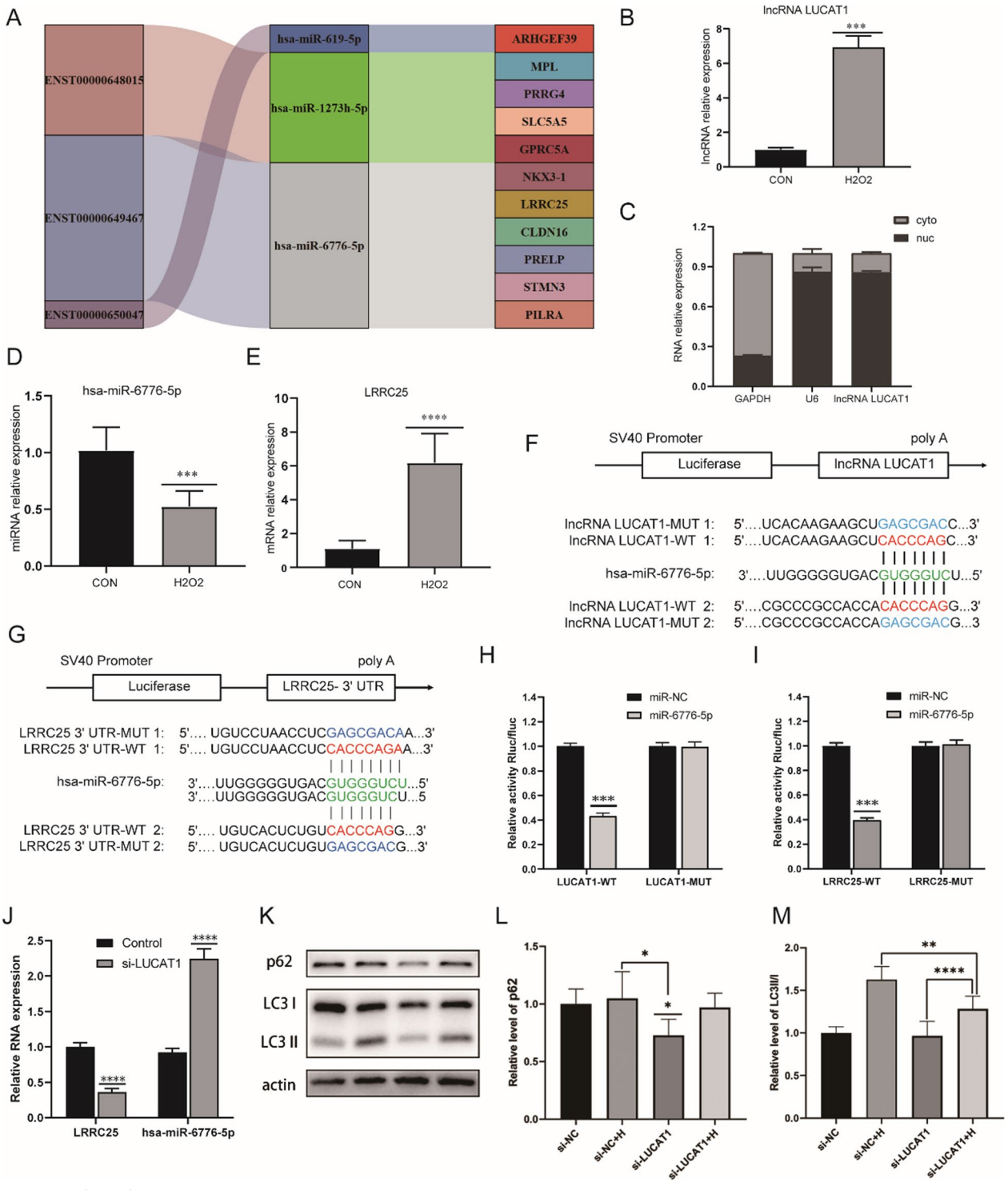

Fig. 6 (See legend on previous page.)

ATG7 (model III), as depicted in (Fig. 8A–C). The ROC curve analysis identified the most effective autophagy-related model for CAD diagnosis (model III) with an AUC of 0.898, demonstrating a sensitivity of 0.854 and a specificity of 0.910. A nomogram model integrating traditional clinical factors-gender, age, BMI, smoking status, alcohol consumption, hypertension, triglycerides, and HDL-C-with expression levels of p62 and ATG7

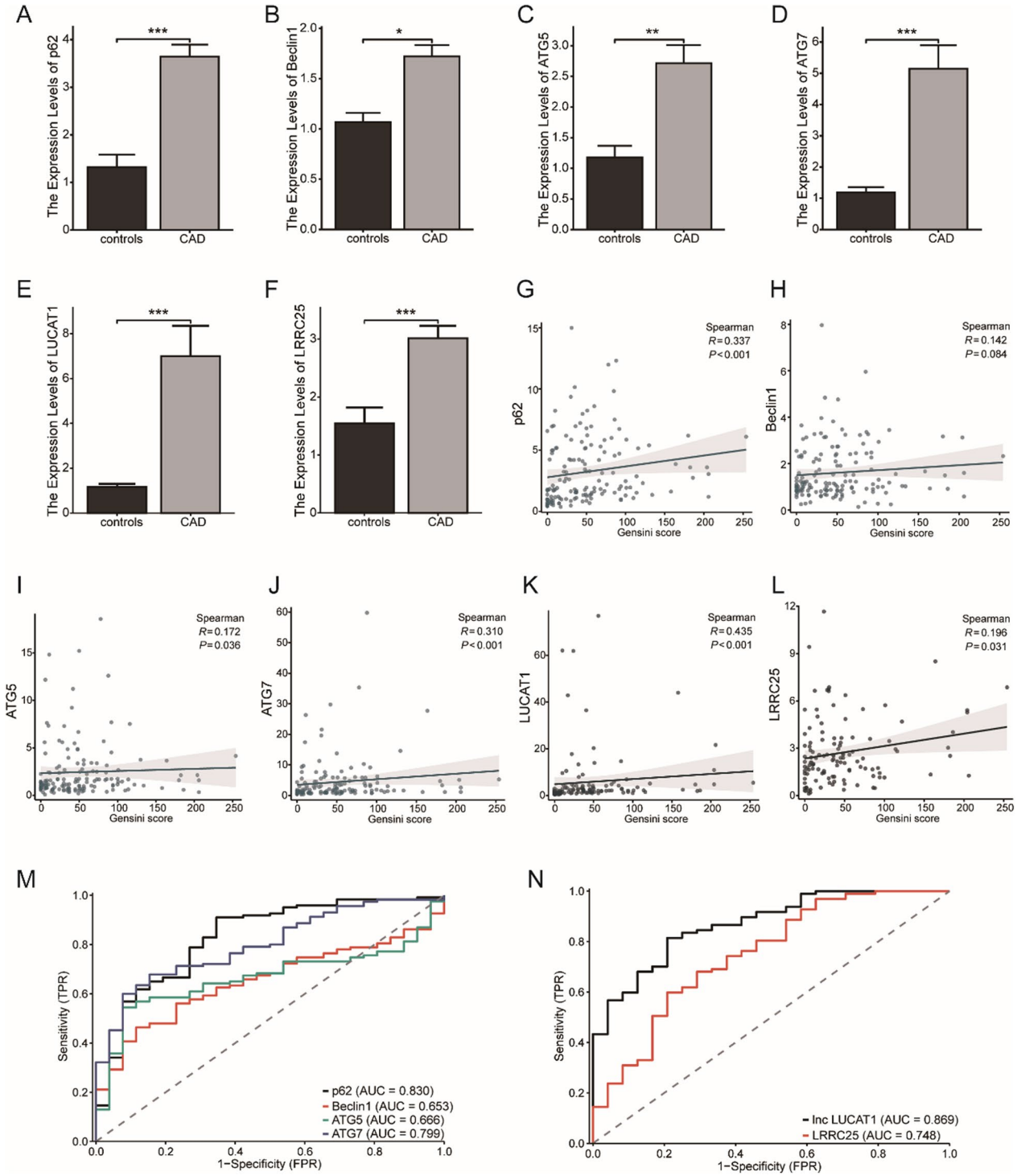

Fig. 7 Validation of autophagy-related RNAs in PBMCs and diagnostic value analysis. The expression levels of **A** p62, **B** Beclin1, **C** ATG5, **D** ATG7 (controls n = 26, CAD n = 123), **E** lncRNA LUCAT1, and **F** LRRC25 (controls n = 24, CAD n = 97) in PBMCs quantified by qPCR. Spearman correlation analysis between Gensini score and **G** p62, **H** Beclin1, **I** ATG5, **J** ATG7 (controls n = 26, CAD n = 123), **K** lncRNA LUCAT1, and **L** LRRC25 (controls n = 24, CAD n = 97), respectively. ROC curves estimate the diagnostic values of **M** p62, Beclin1, ATG5, and ATG7, and **N** lncRNA LUCAT1 and LRRC25. *$P < 0.05$, **$P < 0.01$, ***$P < 0.001$

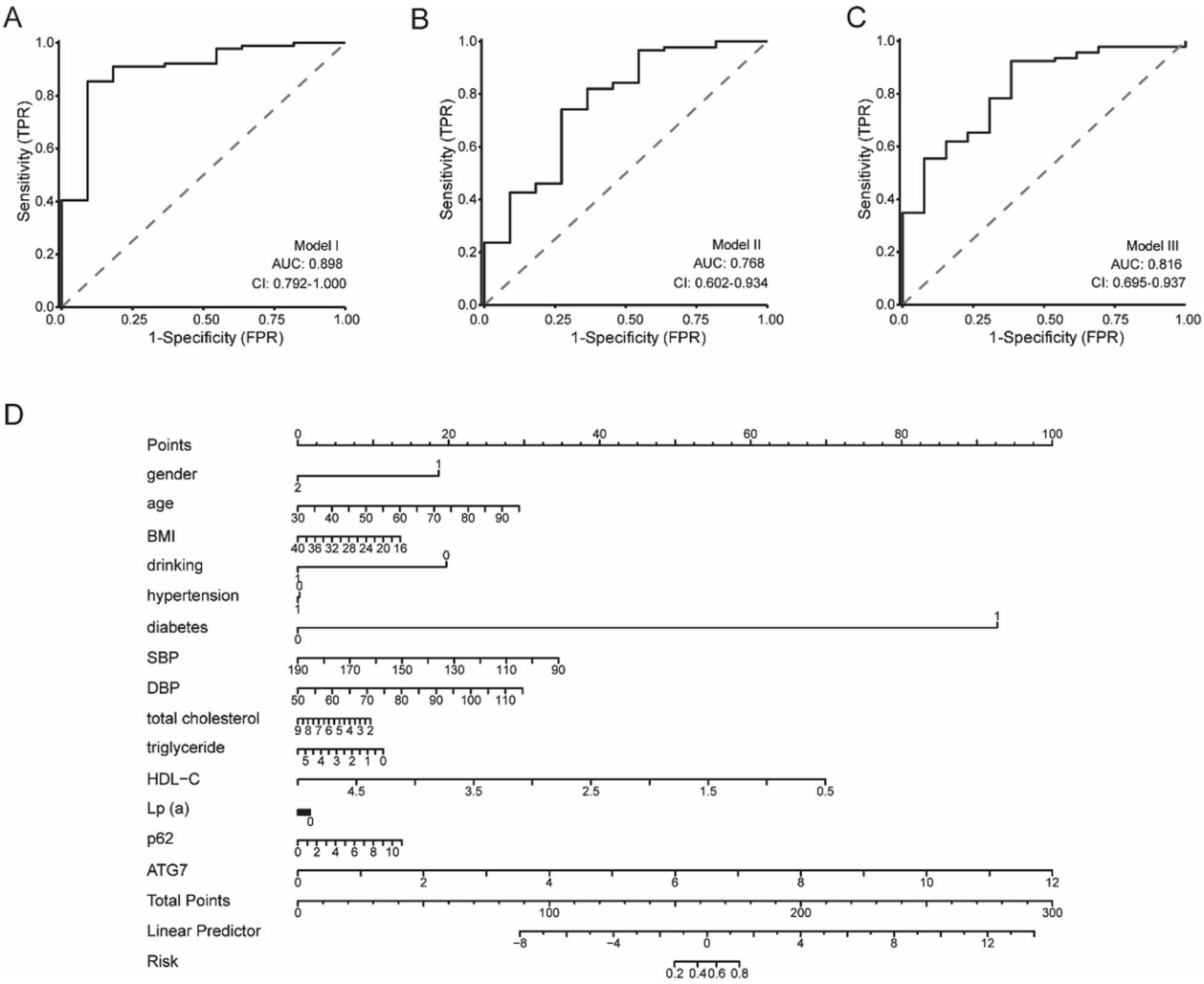

Fig. 8 Receiver operating characteristic curve of the diagnostic validity and nomogram construction. ROC curves estimate the diagnostic values of the **A** diagnostic model I including CRP, lipids parameters, and p62, of the **B** diagnostic model II including CRP, lipids parameters, and ATG7, and of the **C** diagnostic model III including CRP, lipids parameters, p62, and ATG7; **D** construction of nomogram model predicting CAD risk

in PBMCs was developed to predict CAD risk. These findings highlight the superior diagnostic capability of autophagy-related RNAs in detecting CAD (Fig. 8D).

Discussion

CAD is the primary cause of morbidity and mortality globally, typically marked by the gradual, irreversible progression of coronary atherosclerosis [21, 22]. With the formation and progression of intimal plaques, involving multiple cellular dysfunctions and programmed cell death, the coronary artery lumen narrows, impeding blood flow to cardiac tissues and potentially leading to adverse cardiovascular events [23]. Among multiple cellular biological processes functioning in inflammation and atherosclerosis, autophagy is a critical regulator of cardiovascular homeostasis and poses a dual impact on atherosclerosis via modulating cell activities [24–26]. Due to the challenges associated with obtaining human coronary artery specimens, the majority of published studies exploring the interaction between autophagy and atherosclerosis have primarily relied on findings derived from ApoE-/- mouse models. Still, a recent study employing immunohistochemical analysis of human left coronary artery specimens revealed that stenotic lesions group had significantly higher LC3 expression and lower p62 expression compared to the control group [27]. However, to date, no comprehensive studies have reported on the specific autophagy patterns in human coronary atherosclerosis under physiological conditions. In the present study, we observed a progressive reduction in the expression

of ATG5, Beclin1, and LC3 as atherosclerosis advanced pathologically, with the lowest levels detected in stage 3, while p62 expression showed a corresponding increase. As ATG5, Beclin1, and LC3 drive autophagy progression, while p62, as a cargo protein, mediates substrate delivery before ultimately being degraded, the opposing trends observed in this study support the consistent patterns of autophagic alterations. Altogether, our results indicate a sustained impairment of the autophagy process associated with atherosclerosis progression, which is consistent with findings from several animal studies [28, 29]. Initially, dynamic autophagy is expected, as injury and adaptive repair dominate the early stages of atherosclerosis, promoting global autophagy activity to protect against endothelial dysfunction and low-density lipoprotein (LDL) aggregation. During the progressive stages, programmed cell death occurs extensively and gradually, leading to the destruction of cells and their structural and functional inability to sustain autophagy activities [30, 31]. Our findings provide the first comprehensive depiction of the prolonged and impaired autophagy landscape in coronary atherosclerosis, highlighting the potential of preserving normal autophagic activity as a therapeutic target for early CAD intervention.

Furthermore, lncRNAs are a subgroup of RNAs that play a key role in regulating gene expression and major biological processes [32]. First reported in lung cancer [33], numerous studies have highlighted the oncogenic role of lncRNA LUCAT1 in regulating cell proliferation, invasion, and migration in multiple cancers [34]. Prior study have indicated that the expression of LUCAT1 is markedly decreased in the peripheral venous blood of patients with acute myocardial infarction (AMI), and it protects cardiomyocytes against oxidative stress-induced damage via targeting miR-181a-5p [11]. Moreover, reduced expression of LUCAT1 is strongly correlated with the severity and unfavorable clinical outcomes of chronic heart failure (CHF), as it facilitates cardiomyocyte apoptosis through the regulation of the miR-612/HOXA13 axis [12]. Although the role of LUCAT1 in cardiomyocytes has been established in both AMI and CHF, its involvement in the biological regulation of CAD progression, particularly in endothelial cell injury, remains unclear. In our research, we observed a significant upregulation of LUCAT1 in PBMCs from the CAD group compared to the control group, as well as in HACECs subjected to oxidative stress-induced injury. Further analysis confirmed that LUCAT1 demonstrates exceptional potential as a diagnostic biomarker for CAD. The opposite expression trend observed in this study, compared to existing studies, may be attributed to differences in sample sources. While RNA in previous studies was extracted from peripheral blood serum, this study utilized PBMCs. It may also reflect differences arising from the pathological characteristics of the disease itself.

Besides, recent studies defined LRRC25 as an autophagy-associated gene, or the secondary receptor, due to LRRC25 mediating the enhancing interaction of cargo proteins and p62 through direct binding and promoting autophagic-dependent degradation [35, 36]. However, no studies about LRRC25 or hsa-miR-6776-5p on CAD have been reported. Through integrated bioinformatics prediction and algorithm cross-validation, we identified an autophagy-associated lncRNA, lncRNA LUCAT1, that exhibited a significantly high correlation with autophagy-related genes. Supporting the idea that its functional pattern depends on its location, we surmised that LUCAT1 modifies intracellular autophagy response by regulating gene expression via altering the stability or translation of mRNAs in the cytoplasm [37]. Consequently, the downstream hsa-miR-6776-5p/LRRC25 axis was established and a LUCAT1-mediated ceRNA network was constructed in this study. The incomplete binding sites between LUCAT1 and hsa-miR-6776-5p, as well as between hsa-miR-6776-5p and LRRC25, were predicted and validated using dual-luciferase reporter assay. The expression levels of hsa-miR-6776-5p and LRRC25 were significantly altered following LUCAT1 interference, proving the intermolecular regulatory relationships that characterize the ceRNA mechanism. In our present study, LUCAT1 facilitated autophagy activation in HCAEC under oxidative stress, while impaired autophagy excitation was detected in LUCAT1 knockdown-HCAECs. Given that elevated autophagy protects HCAECs against oxidative stress, the lncRNA LUCAT1/hsa-miR-6776-5p/LRRC25 axis may serve as a promising targets for early treatment of CAD.

Despite the availability of advanced invasive clinical methods for managing high-risk CAD patients, early-stage CAD often remains undiagnosed due to the limited sensitivity and specificity of early diagnostic strategies [38]. Consequently, the identification of reliable and robust biomarkers for the early diagnosis of CAD are both invaluable and urgently needed. Several studies have corroborated the diagnostic values of autophagy-related indicators for CAD. ATG5 mRNA levels were reduced in the peripheral blood [39], while the protein expression of ATG5 was elevated in the plasma of CAD patients than in healthy subjects [40]. Likewise, the expression levels of LC3 in peripheral leucocytes and Beclin1 in serum were reported to be significantly lower in CAD patients [41, 42]. However, the clinical relevance of autophagy markers requires further investigation. In our study, we comprehensively evaluated the diagnostic performance of autophagy markers in CAD using PBMC-derived samples. The expression quantification levels of p62, Beclin1,

ATG5, ATG7, lncRNA LUCAT1, and LRRC25 were markedly decreased in PBMCs from CAD patients. The subsequent correlation analysis revealed a significant positive association between those autophagy-related indicators and the severity of coronary artery stenosis. ROC curve analysis further supported their superior AUC values, underscoring the significant translational value of this study. These observed variations likely shed light on the role of autophagy in the progression of coronary atherosclerosis and its intricate interplay with the disease pathophysiology. Among clinical lipid parameters, elevated triglycerides and reduced HDL-C, rather than abnormalities in total cholesterol or LDL-C levels, are reported to be strongly correlated with CAD risk [43, 44]. Additionally, the inflammatory biomarker CRP is widely utilized in cardiovascular risk assessments due to its strong correlation with cardiovascular events [45]. Building on this evidence, our ROC curve analysis identified that autophagy-related p62 serves as a more prominent biomarker for CAD diagnosis in PBMCs. By integrating these findings with established CAD risk factors and validated diagnostic models, we developed a nomogram that provides an intuitive and practical tool for assessing individual CAD risk [46]. The nomogram demonstrated excellent accuracy and reliability in differentiating CAD patients from healthy individuals. Specifically, for each patient, a total score is generated by summing the values assigned to each independent variable, which directly correlates with the predicted risk of CAD occurrence. In conclusion, our study identified four autophagy markers—p62, ATG7, lncRNA LUCAT1, and LRRC25—in PBMCs are credible biomarkers and promising targets for CAD diagnosis. Our study integrates the autophagic process into the clinical diagnosis and treatment of CAD by elucidating its role in the pathophysiology of the disease. Ultimately, these insights could contribute to improving the efficacy of existing therapeutic strategies and expanding options for clinical intervention.

The consistent trend of LUCAT1 expression observed in PBMCs and the cellular model has captured our attention. This may reflect independent differential expression events within two distinct cellular systems involved in the disease, or it could provide evidence of the interaction between PBMCs and endothelial cells during the atherosclerosis process, particularly mediated by exosomal communication. PBMCs are a vital component of the immune system, and few studies have demonstrated cellular interactions between PBMCs and endothelial cells through limited and ambiguous mechanisms. For instance, PBMCs derived from patients with acute Kawasaki disease can induce excessive autophagy in HCAECs through cytokine secretion during co-culture, which was partially mitigated by 3-MA [47]. Another study found that autophagy levels in PBMCs were elevated in patients with type 1 diabetes, promoting leukocyte-endothelium interactions through adhesion [48]. However, the crosstalk interactions and specific mechanisms between PBMCs and HCAECs during CAD progression remain unexplored. The future research will focus on investigating the relationship between changes in autophagy-related genes in PBMCs and HCAECs, as well as their underlying mechanisms.

Several limitations were noted in this study. First, larger sample sizes of available PBMCs from both CAD patients and healthy individuals are required for further external validation of differential expression and diagnostic efficiency. Second, the absence of clinical prognosis-related data precludes the determination of the predictive values of the identified biomarkers. Lastly, further experiments are needed to confirm the lncRNA LUCAT1/hsa-miR-6776-5p/LRRC25 axis and their modulation on autophagy. Additionally, more comprehensive functional experiments should be conducted in vitro and in vivo.

Conclusions

In this study, we characterized the dynamic disruption of the autophagy landscape linked to the progression of human coronary atherosclerosis and unveiled the transcriptional profile associated with endothelial cell injury. Furthermore, we identified the lncRNA LUCAT1/hsa-miR-6776-5p/LRRC25 axis, which enhanced autophagy and conferred protection against cellular damage. Notably, we recognized p62, ATG7, lncRNA LUCAT1, and LRRC25 as reliable autophagy-related diagnostic biomarkers in circulating PBMCs, correlating with coronary artery disease (CAD) severity. Collectively, our findings furnish novel insights into the intricate autophagy landscape at various levels of coronary atherosclerosis and propose potential diagnostic biomarkers, strategies for diagnosis, and a theoretical foundation for managing CAD patients.

Abbreviations

3-MA	3-Methyladenine
ATG5	Autophagy related 5
ATG7	Autophagy related 7
AUC	Area under the curve
CAD	Coronary artery disease
CCK-8	Cell counting kit-8
ceRNA	Competing endogenous RNA
CQ	Chloroquine
DE	Differentially expressed

ECs	Endothelial cells
GO	Gene ontology
H_2O_2	Hydrogen peroxide
HCAECs	Human coronary artery endothelial cells
IHC	Immunohistochemistry
KEGG	Kyoto Encyclopedia of Genes and Genomes
LC3	Microtubule associated protein 1 light chain 3
lncRNAs	Long noncoding RNAs
LRRC25	Leucine rich repeat containing 25
LUCAT1	Lung cancer associated transcript 1
SQSTM1/p62	Sequestosome 1
PBMCs	Peripheral blood mononuclear cells
PPI	Protein–protein interaction
qPCR	Quantitative real-time PCR
ROC	Receiver operating characteristic
ROS	Reactive oxygen species

Supplementary Information

The online version contains supplementary material available at https://doi.org/10.1186/s12967-024-05966-2.

Supplementary Material 1: Supp Figure 1. Principal component analysis of the lncRNA transcriptome and functional enrichment analysis of down-regulated lncRNAs. **A** PCA of the lncRNA transcriptome of HCAECs from the control and H_2O_2 groups. **B** Three-dimensional PCA of the lncRNA transcriptome of HCAECs from the control and H_2O_2 groups. **C** The top 30 enriched terms associated with the BP, CC, and MF in GO analysis of down-regulated lncRNAs. **D** The top 20 enriched KEGG pathways of down-regulated lncRNAs. PCA, principal component analysis; GO, Geno Ontology; BP, biological process; CC, cellular component; MF, molecular function; KEGG, Kyoto Encyclopedia of Genes and Genomes. Supp Figure 2. PPI network construction and hub genes identification. **A** A PPI network extracted by the first-ranking MCODE plugin in Cytoscape. **B** The lower-ranking modules extracted by the MCODE plugin in Cytoscape. **C** The intersection of hub genes calculated by MNC, MCC, EPC, DMNC, Closeness, Radiality, and Betweenness. **D** A network of the top 15 nodes ranked by MCC. **A**, **B**The blue ellipse indicates down-regulated mRNAs, and the pink ellipse indicates up-regulated mRNAs. The edges refer to the interaction between two nodes, and the degree of the PPI network means the number of edges in one node. PPI, Protein–Protein Interaction. Supp Figure 3. ceRNA network construction. **A** The top 300 predicted DElncRNAs-miRNAs interaction network. **B** A ceRNA network of lncRNA-miRNA-mRNA. The blue rhombus indicates down-regulated lncRNAs, the orange rhombus indicates up-regulated lncRNAs, the green polygon indicates down-regulated mRNAs, the bluish violet polygon indicates up-regulated mRNAs and the purple rectangle indicates predicted miRNAs. DElncRNAs, differentially expressed long noncoding RNAs; ceRNA, competing endogenous RNAs.

Supplementary Material 2.

Supplementary Material 3.

Supplementary Material 4.

Supplementary Material 5.

Supplementary Material 6.

Supplementary Material 7.

Supplementary Material 8.

Acknowledgements
This study received support from the National Natural Science Foundation of China and the Priority Academic Development Programme of the Jiangsu Higher Education Institutions. Dr. Enzhi Jia is an Assistant Fellow at the Collaborative Innovation Center for Cardiovascular Disease Translational Medicine. We would like to thank the Core Facility of The First Affiliated Hospital of Nanjing Medical University for its help in the detection of experimental samples.

Author contributions
As the guarantor, Enzhi Jia, Xiumei Chen, and Fenghui An conceived this study. Yanjun Wang, Xin Zhang, and Mengmeng Ren drafted and revised the manuscript. Yanjun Wang, Xin Zhang, and Mengmeng Ren performed experiments. Shu He, Hanxiao Zhou, Hengjie Bie, Mengyang Duan, and Zhiyuan Chen enrolled participants. Qiaowei Jia, Boyu Chi, Xiongkang Gan, Chengcheng Li, and Yahong Fu conducted the statistical analysis. Sheng Zhang and Qian Zhang coordinated this study.

Funding
This study received support from the National Natural Science Foundation of China (No. 81970302), the Priority Academic Program Development of Jiangsu Higher Education Institutions, the Postgraduate Research & Practice Innovation Program of Jiangsu Province(No. JX10214100), and the Ten-zan's Cedar Doctor Training Program(No.yl2022py07).

Data availability
The datasets used and/or analyzed during the current study are available from the corresponding author upon reasonable request.

Declarations

Ethics approval and consent to participate
The methods were performed following the approved guidelines, and all experimental protocols were approved by the ethics committee of Nanjing Medical University and the First Affiliated Hospital of Nanjing Medical University.

Consent for publication
All authors have read and approved the manuscript.

Competing interests
No potential competing interests was associated with this manuscript.

Author details
[1]Department of Cardiovascular Medicine, The First Affiliated Hospital of Nanjing Medical University, Guangzhou Road 300, Nanjing 210029, Jiangsu, China. [2]Department of Geriatric, The First Affiliated Hospital of Nanjing Medical University, Guangzhou Road 300, Nanjing 210029, Jiangsu, China. [3]Department of Critical Care Medicine, The Friendship Hospital of Ili Kazakh Autonomous Prefecture, Yining 835000, Xinjiang, China.

Received: 10 September 2024 Accepted: 11 December 2024
Published online: 31 December 2024

References

1. Mensah GA, Fuster V, Murray CJL, Roth GA. Global burden of cardiovascular D, risks C: global burden of cardiovascular diseases and risks, 1990–2022. J Am Coll Cardiol. 2023;82:2350–473.
2. Virani SS, Newby LK, Arnold SV, Bittner V, Brewer LC, Demeter SH, Dixon DL, Fearon WF, Hess B, Johnson HM, et al. 2023 AHA/ACC/ACCP/ASPC/NLA/PCNA Guideline for the Management of Patients With Chronic Coronary Disease: a report of the American Heart Association/American College of Cardiology Joint Committee on Clinical Practice Guidelines. Circulation. 2023;148:e9–119.
3. Malakar AK, Choudhury D, Halder B, Paul P, Uddin A, Chakraborty S. A review on coronary artery disease, its risk factors, and therapeutics. J Cell Physiol. 2019;234:16812–23.
4. Klionsky DJ, Petroni G, Amaravadi RK, Baehrecke EH, Ballabio A, Boya P, Bravo-San Pedro JM, Cadwell K, Cecconi F, Choi AMK, et al. Autophagy in major human diseases. EMBO J. 2021;40: e108863.
5. Liu S, Yao S, Yang H, Liu S, Wang Y. Autophagy: regulator of cell death. Cell Death Dis. 2023;14:648.

6. Kheloufi M, Vion AC, Hammoutene A, Poisson J, Lasselin J, Devue C, Pic I, Dupont N, Busse J, Stark K, et al. Endothelial autophagic flux hampers atherosclerotic lesion development. Autophagy. 2018;14:173–5.
7. Xiao S, Song X, Zheng M, Cao X, Ai G, Li B, Zhao G, Yuan H. Interleukin-37 ameliorates atherosclerosis by regulating autophagy-mediated endothelial cell apoptosis and inflammation. Int Immunopharmacol. 2023;118:110098.
8. Perrotta P, Van der Veken B, Van Der Veken P, Pintelon I, Roosens L, Adriaenssens E, Timmerman V, Guns PJ, De Meyer GRY, Martinet W. Partial inhibition of glycolysis reduces atherogenesis independent of intraplaque neovascularization in mice. Arterioscler Thromb Vasc Biol. 2020;40:1168–81.
9. Meng Q, Pu L, Qi M, Li S, Sun B, Wang Y, Liu B, Li F. Laminar shear stress inhibits inflammation by activating autophagy in human aortic endothelial cells through HMGB1 nuclear translocation. Commun Biol. 2022;5:425.
10. Fan Y, Zhang Y, Zhao H, Liu W, Xu W, Jiang L, Xu R, Zheng Y, Tang X, Li X, et al. lncR-GAS5 upregulates the splicing factor SRSF10 to impair endothelial autophagy, leading to atherogenesis. Front Med. 2023;17:317–29.
11. Xiao SH, Wang Y, Cao X, Su Z. Long non-coding RNA LUCAT1 inhibits myocardial oxidative stress and apoptosis after myocardial infarction via targeting microRNA-181a-5p. Bioengineered. 2021;12:4546–55.
12. Li T, Qian D, Guoyan J, Lei Z. Downregulated long noncoding RNA LUCAT1 inhibited proliferation and promoted apoptosis of cardiomyocyte via miR-612/HOXA13 pathway in chronic heart failure. Eur Rev Med Pharmacol Sci. 2020;24:385–95.
13. Wu H, Liu T, Qi J, Qin C, Zhu Q. Four autophagy-related lncRNAs predict the prognosis of HCC through coexpression and ceRNA mechanism. Biomed Res Int. 2020;2020:3801748.
14. Zhou Y, Yuan J, Fan Y, An F, Chen J, Zhang Y, Jin J, Gu M, Mao Z, Sun H, et al. Proteomic landscape of human coronary artery atherosclerosis. Int J Mol Med. 2020;46:371–83.
15. Zhou Y, Zhou H, Hua L, Hou C, Jia Q, Chen J, Zhang S, Wang Y, He S, Jia E. Verification of ferroptosis and pyroptosis and identification of PTGS2 as the hub gene in human coronary artery atherosclerosis. Free Radic Biol Med. 2021;171:55–68.
16. Lu H, Zhao S, Tian D, Chen Y, Ma J, Ge M, Zeng M, Jin H. A clinical strategy to improve the diagnostic performance of 3T non-contrast coronary MRA and noninvasively evaluate coronary distensibility: combination of diastole and systole imaging. J Cardiovasc Magn Reson. 2023;25:67.
17. Aksu F, Ahmed SA. Gensini score's severity and its relationship with risk factors for coronary artery disease among patients who underwent angiography in somalia's largest PCI centre. Int J Gen Med. 2024;17:187–92.
18. Barth S, Glick D, Macleod KF. Autophagy: assays and artifacts. J Pathol. 2010;221:117–24.
19. Lewandowski JP, Lee JC, Hwang T, Sunwoo H, Goldstein JM, Groff AF, Chang NP, Mallard W, Williams A, Henao-Meija J, et al. The Firre locus produces a trans-acting RNA molecule that functions in hematopoiesis. Nat Commun. 2019;10:5137.
20. Du Y, Duan T, Feng Y, Liu Q, Lin M, Cui J, Wang RF. LRRC25 inhibits type I IFN signaling by targeting ISG15-associated RIG-I for autophagic degradation. EMBO J. 2018;37:351–66.
21. GBD 2019 Diseases and Injuries Collaborators. Global burden of 369 diseases and injuries in 204 countries and territories, 1990–2019: a systematic analysis for the Global Burden of Disease Study 2019. Lancet. 2020;396:1204–22.
22. Virani SS, Alonso A, Aparicio HJ, Benjamin EJ, Bittencourt MS, Callaway CW, Carson AP, Chamberlain AM, Cheng S, Delling FN, et al. Heart disease and stroke statistics-2021 update: a report from the American Heart Association. Circulation. 2021;143:e254–743.
23. Stakhneva EM, Striukova EV, Ragino YI. Proteomic studies of blood and vascular wall in atherosclerosis. Int J Mol Sci. 2021;22:13267.
24. Pi S, Mao L, Chen J, Shi H, Liu Y, Guo X, Li Y, Zhou L, He H, Yu C, et al. The P2RY12 receptor promotes VSMC-derived foam cell formation by inhibiting autophagy in advanced atherosclerosis. Autophagy. 2021;17:980–1000.
25. Yuan P, Hu Q, He X, Long Y, Song X, Wu F, He Y, Zhou X. Laminar flow inhibits the Hippo/YAP pathway via autophagy and SIRT1-mediated deacetylation against atherosclerosis. Cell Death Dis. 2020;11:141.
26. Evans TD, Jeong SJ, Zhang X, Sergin I, Razani B. TFEB and trehalose drive the macrophage autophagy-lysosome system to protect against atherosclerosis. Autophagy. 2018;14:724–6.
27. Li F, Peng J, Lu Y, Zhou M, Liang J, Le C, Ding J, Wang J, Dai J, Wan C, et al. Blockade of CXCR4 promotes macrophage autophagy through the PI3K/AKT/mTOR pathway to alleviate coronary heart disease. Int J Cardiol. 2023;392:131303.
28. Lu H, Fan Y, Qiao C, Liang W, Hu W, Zhu T, Zhang J, Chen YE. TFEB inhibits endothelial cell inflammation and reduces atherosclerosis. Sci Signal. 2017;10: eaah4214.
29. Zhang H, Ge S, Ni B, He K, Zhu P, Wu X, Shao Y. Augmenting ATG14 alleviates atherosclerosis and inhibits inflammation via promotion of autophagosome-lysosome fusion in macrophages. Autophagy. 2021;17:4218–30.
30. Li J, Meng Q, Fu Y, Yu X, Ji T, Chao Y, Chen Q, Li Y, Bian H. Novel insights: dynamic foam cells derived from the macrophage in atherosclerosis. J Cell Physiol. 2021;236:6154–67.
31. Navas-Madronal M, Castelblanco E, Camacho M, Consegal M, Ramirez-Morros A, Sarrias MR, Perez P, Alonso N, Galan M, Mauricio D. Role of the scavenger receptor CD36 in accelerated diabetic atherosclerosis. Int J Mol Sci. 2020;21:7360.
32. Ransohoff JD, Wei Y, Khavari PA. The functions and unique features of long intergenic non-coding RNA. Nat Rev Mol Cell Biol. 2018;19:143–57.
33. Sun Y, Jin SD, Zhu Q, Han L, Feng J, Lu XY, Wang W, Wang F, Guo RH. Long non-coding RNA LUCAT1 is associated with poor prognosis in human non-small lung cancer and regulates cell proliferation via epigenetically repressing p21 and p57 expression. Oncotarget. 2017;8:28297–311.
34. Xing C, Sun SG, Yue ZQ, Bai F. Role of lncRNA LUCAT1 in cancer. Biomed Pharmacother. 2021;134:111158.
35. Feng Y, Duan T, Du Y, Jin S, Wang M, Cui J, Wang RF. LRRC25 functions as an inhibitor of NF-kappaB signaling pathway by promoting p65/RelA for autophagic degradation. Sci Rep. 2017;7:13448.
36. Xian H, Yang S, Jin S, Zhang Y, Cui J. LRRC59 modulates type I interferon signaling by restraining the SQSTM1/p62-mediated autophagic degradation of pattern recognition receptor DDX58/RIG-I. Autophagy. 2020;16:408–18.
37. Statello L, Guo CJ, Chen LL, Huarte M. Gene regulation by long non-coding RNAs and its biological functions. Nat Rev Mol Cell Biol. 2021;22:96–118.
38. Yang Y, Cai Y, Wu G, Chen X, Liu Y, Wang X, Yu J, Li C, Chen X, Jose PA, et al. Plasma long non-coding RNA, CoroMarker, a novel biomarker for diagnosis of coronary artery disease. Clin Sci. 2015;129:675–85.
39. Ebadi N, Ghafouri-Fard S, Taheri M, Arsang-Jang S, Parsa SA, Omrani MD. Dysregulation of autophagy-related lncRNAs in peripheral blood of coronary artery disease patients. Eur J Pharmacol. 2020;867:172852.
40. Kaplan O, Demircan G. Relationship of autophagy and apoptosis with total occlusion of coronary arteries. Med Sci Monit. 2018;24:6984–8.
41. Naguib M, Tarabay A, ElSaraf N, Rashed L, ElMeligy A. Beclin1 circulating level as predictor of carotid intima-media thickness in patients with type 2 diabetes mellitus. Medicine. 2021;100: e26630.
42. Wu G, Wei G, Huang J, Pang S, Liu L, Yan B. Decreased gene expression of LC3 in peripheral leucocytes of patients with coronary artery disease. Eur J Clin Invest. 2011;41:958–63.
43. Chen Z, Chen G, Qin H, Cai Z, Huang J, Chen H, Wu W, Chen Z, Wu S, Chen Y. Higher triglyceride to high-density lipoprotein cholesterol ratio increases cardiovascular risk: 10-year prospective study in a cohort of Chinese adults. J Diabetes Investig. 2020;11:475–81.
44. Di Giorgi N, Michelucci E, Smit JM, Scholte A, El Mahdiui M, Knuuti J, Buechel RR, Teresinska A, Pizzi MN, Roque A, et al. A specific plasma lipid signature associated with high triglycerides and low HDL cholesterol identifies residual CAD risk in patients with chronic coronary syndrome. Atherosclerosis. 2021;339:1–11.
45. Li J, Taylor AM, Manichaikul A, Angle JF, Shi W. Reticulocalbin 2 as a potential biomarker and therapeutic target for atherosclerosis. Cells. 2022;11:1107.
46. Zhou LQ, Liu C, Zou Y, Chen ZQ. Development and verification of the nomogram for dilated cardiomyopathy gene diagnosis. Sci Rep. 2022;12:8908.

47. Qin J, Zheng Y, Ding Y, Huang C, Hou M, Li M, Qian G, Lv H. Co-culture of peripheral blood mononuclear cell (PBMC) and human coronary artery endothelial cell (HCAEC) reveals the important role of autophagy implicated in Kawasaki disease. Transl Pediatr. 2021;10:3140–50.
48. Canet F, Diaz-Pozo P, Luna-Marco C, Fernandez-Reyes M, Vezza T, Marti M, Salazar JD, Roldan I, Morillas C, Rovira-Llopis S, et al. Mitochondrial redox impairment and enhanced autophagy in peripheral blood mononuclear cells from type 1 diabetic patients. Redox Biol. 2022;58:102551.

Publisher's Note